Supplementary Information

A new preparation of bifunctional crystalline heterogeneous copper electrocatalyst by electrodeposition using a robson-type macrocyclic dinuclear copper complex for efficient hydrogen and oxygen evolution from water

Samit Majumder,*[a] Ashraf Abdel Haleem,[a,c] Perumandla Nagaraju[a] and Yoshinori Naruta*[a,b]

[a] Center for Chemical Energy Conversion Research and Institute of Science and Technology Research, Chubu University, Kasugai 487–8501, Japan
[b] JST, Kawaguchi, Saitama, 332-0012, Japan
[c] Department of Engineering Mathematics and Physics, Faculty of Engineering, Fayoum University, Egypt

* E-mail for Y. N: naruta@isc.chubu.ac.jp

E-mail for S. M: smaj@isc.chubu.ac.jp, samitmaj@gmail.com

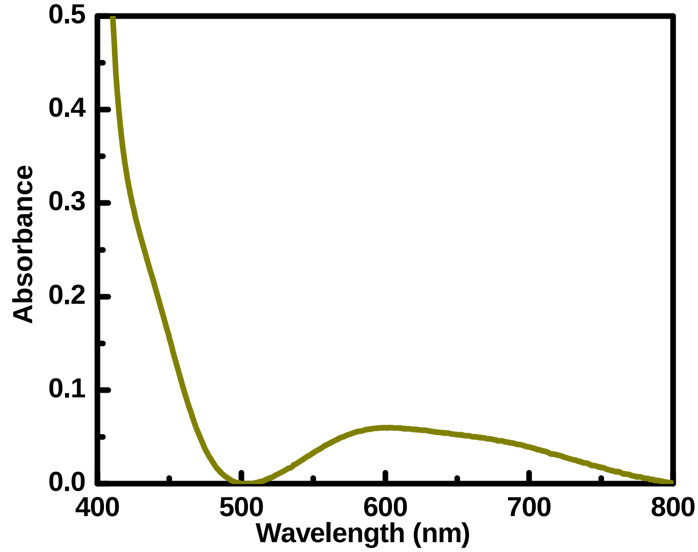

Figure S1. Visible spectra of 0.6 mM of **Cu_2L** in 0.1 M NaBi at pH 9.2.

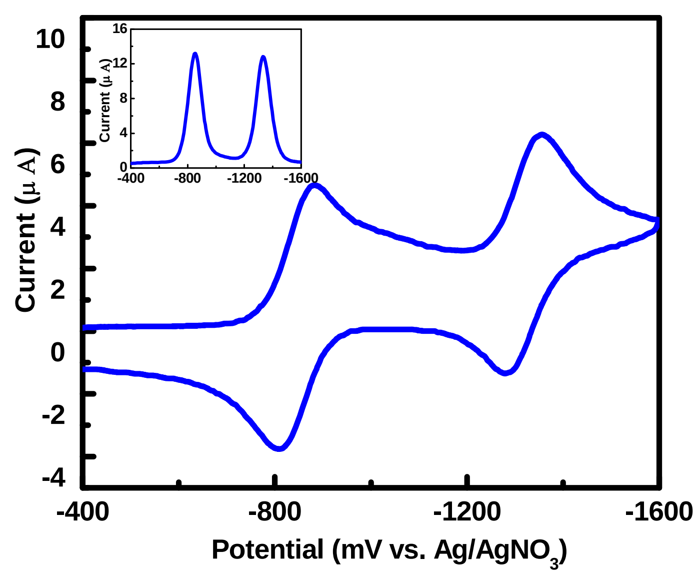

Figure S2. Cyclic voltammogram of **Cu_2L**. Inset shows square wave voltammogram. Conditions; Solvent, dimethylsulphoxide; Sweep speed, 50 mV/s; Working electrode, glassy carbon; Counter electrode, Pt; Reference electrode, $Ag/AgNO_3$.

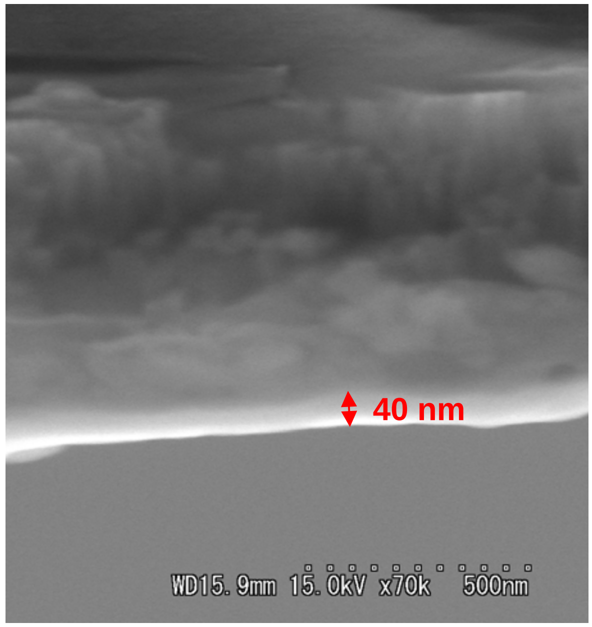

Figure S3. The cross-sectional SEM image of the electrodeposited film H_2-Cu_2Cat on FTO.

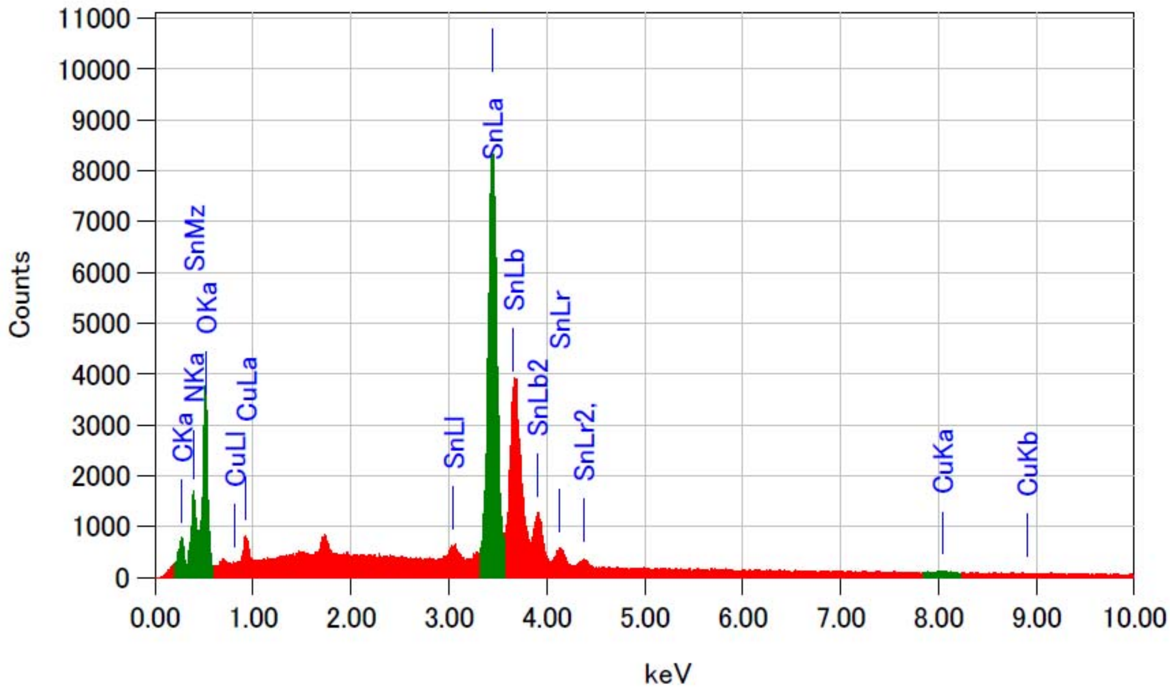

Figure S4. EDX spectrum of the electrodeposited film H_2-Cu_2Cat on FTO.

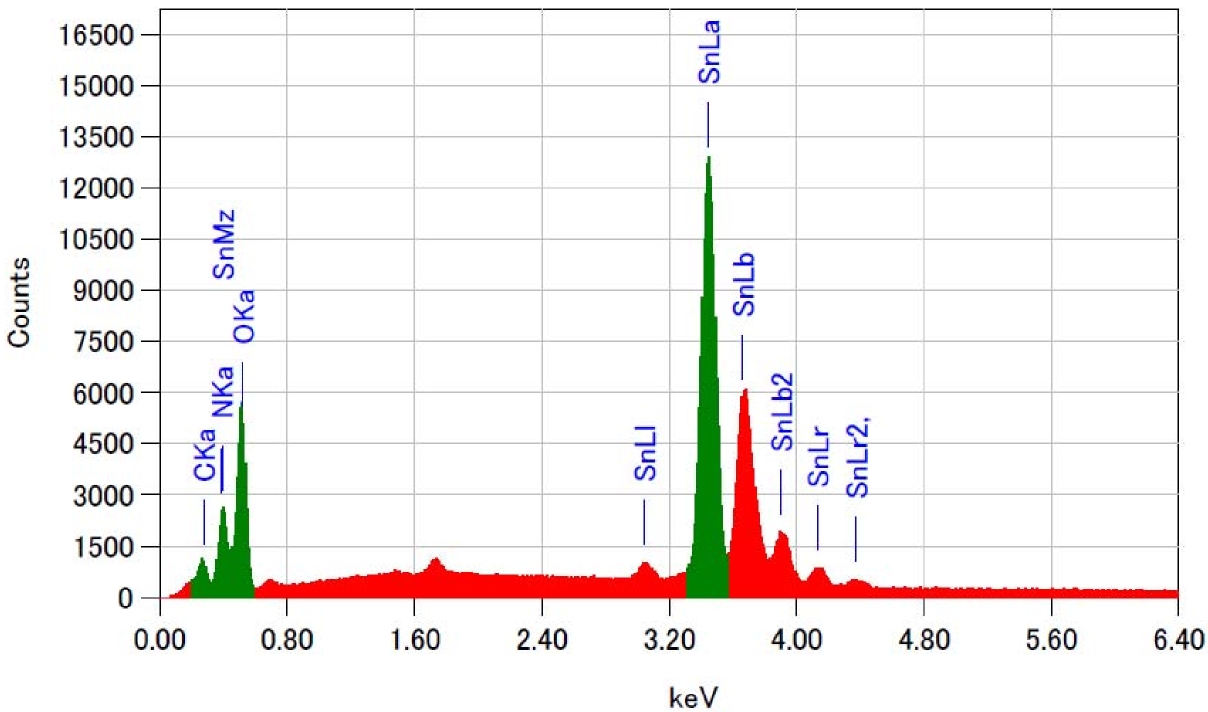

Figure S5. EDX spectrum of a bare FTO.

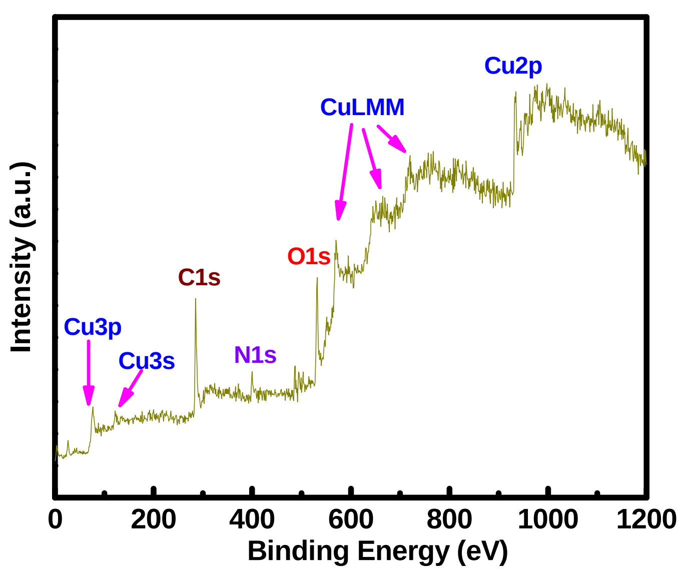

Figure S6. XPS survey data of the H_2-Cu_2Cat on FTO.

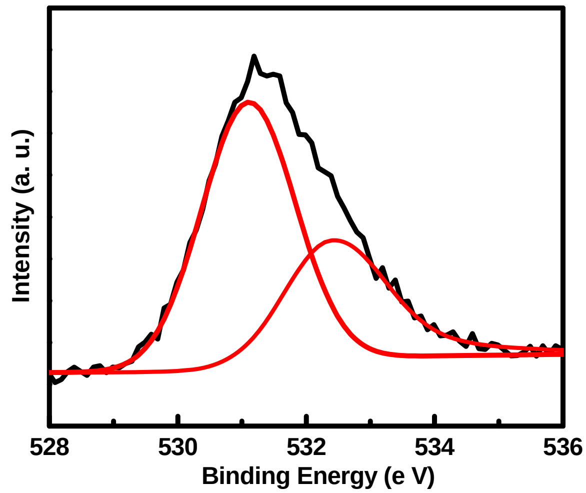

Figure S7. Observed (black) and deconvoluted peaks (red) of O1s in high-resolution XPS scan.

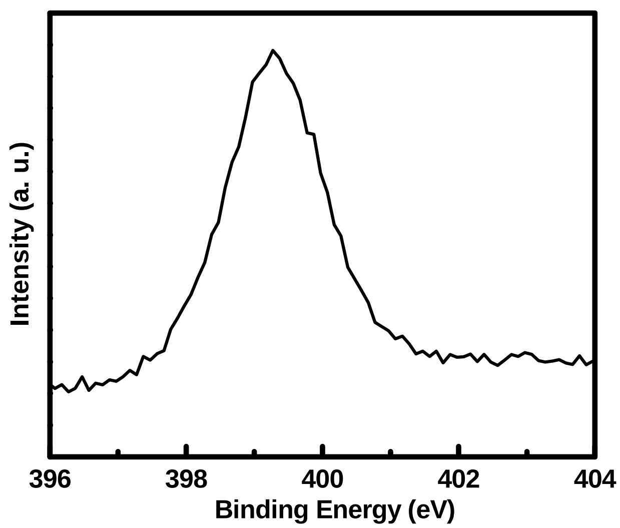

Figure S8. High-resolution XPS scan centered on the N1s peak.

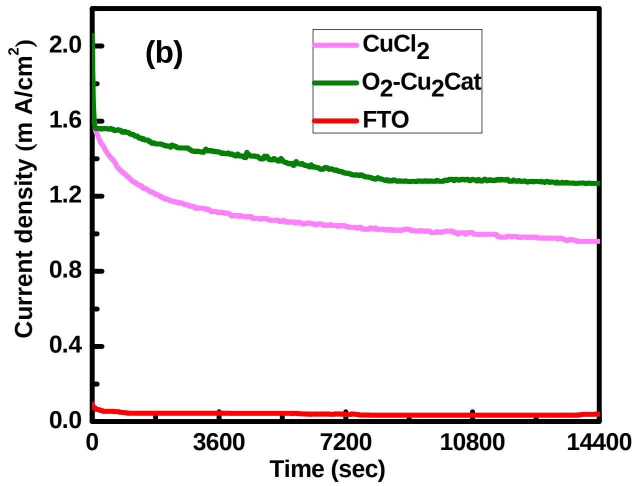

Figure S9. CPE at +1.2 V (*vs.* Ag/AgCl) for the film O_2-Cu_2Cat, bare FTO and electrodeposited film from $CuCl_2$ in 0.1 M NaBi solution of pH 9.2.

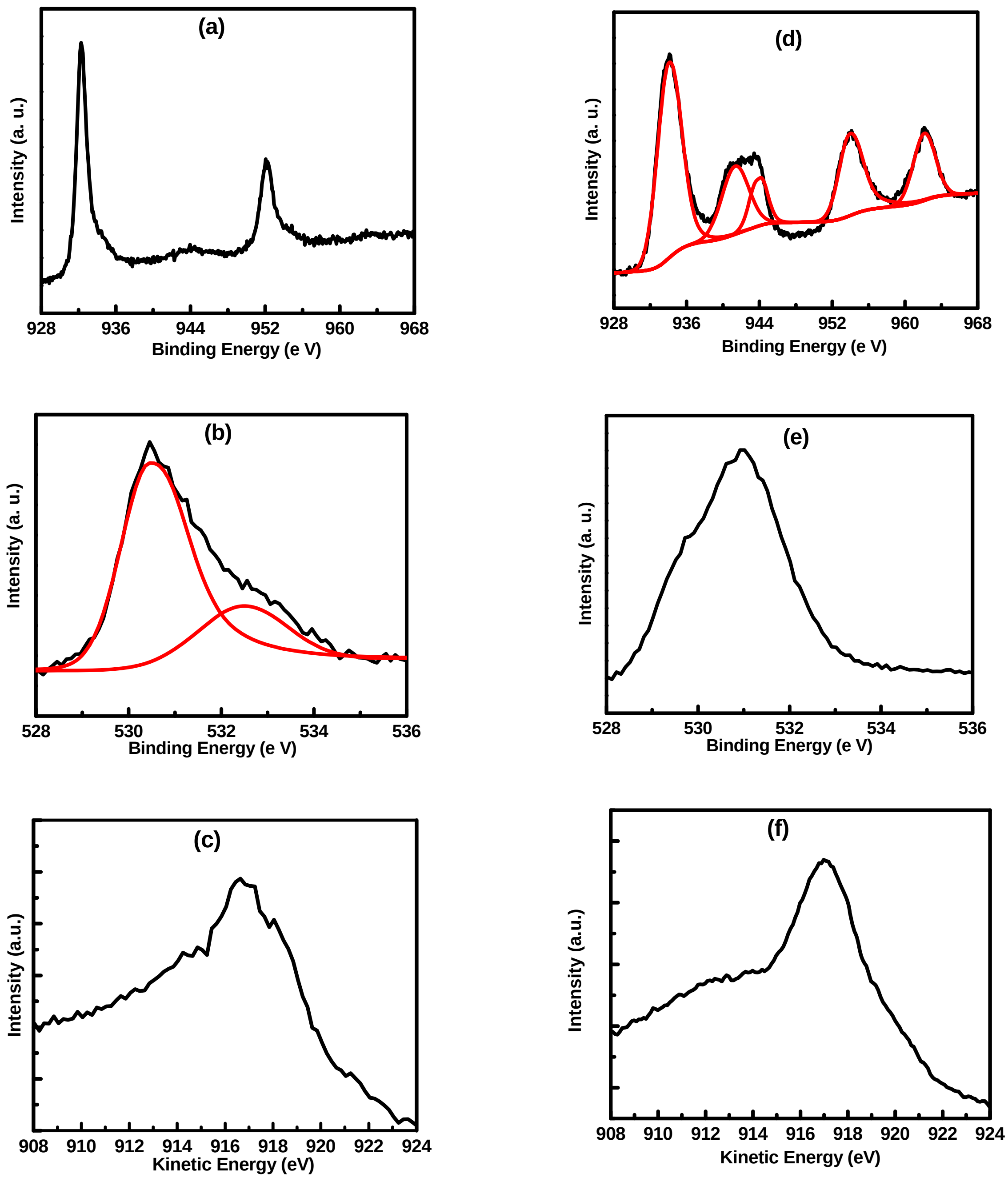

Figure S10. High resolution XPS of Cu2p, O1s and CuLMM region for H_2-Cu_2Cat (a–c) and O_2-Cu_2Cat (d–f) after 4 hr controlled potential electrolysis in 0.1 M NaBi solution at pH 9.2 under an applied potential of –1.20 and +1.20 V *vs*. Ag/AgCl, respectively [Observed (black) and deconvoluted peaks (red)].

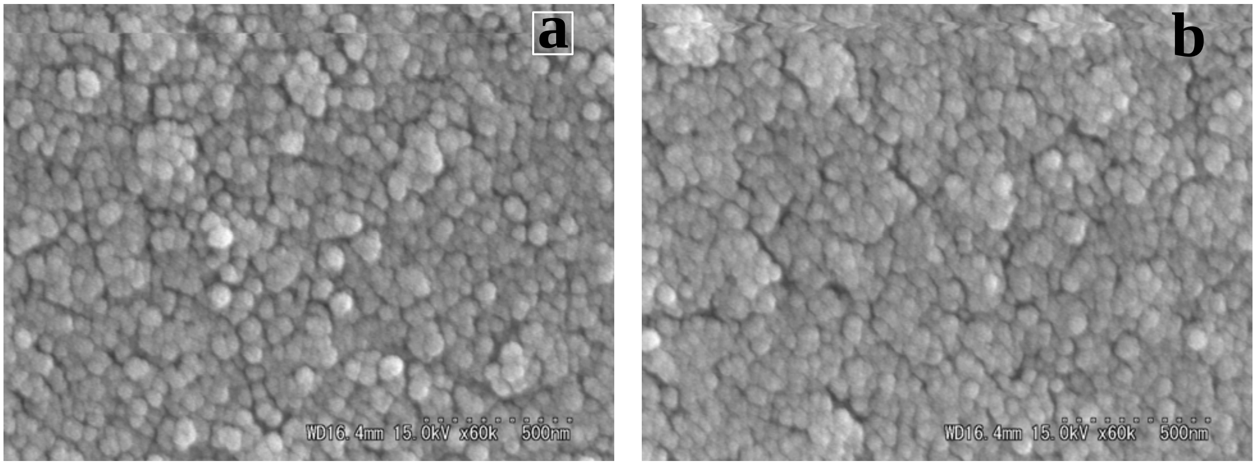

Figure S11. SEM image of (a) H_2-Cu_2Cat film and (b) O_2-Cu_2Cat after 4 hr controlled potential electrolysis in 0.1 M NaBi solution at pH 9.2 under applied potentials of –1.20 V and +1.20 V *vs*. Ag/AgCl, respectively.

Table S1 Comparison of the HER activities of copper-based electrocatalysts

Catalyst	Type of catalyst	Onset potential, V *vs.* NHE; overpotential, mV	Current density *j*, mA cm^{-2}	Overpotential, mV at the corresponding *j*	Electrolytes and pH	Tafel slope, mV dec^{-1}	Base electrode	Reference
H_2-Cu_2Cat from **Cu_2L**	Bifunctional	–0.710; 168	0.1, 1	210, ~440	0.1 M NaBi, 9.2	175	FTO	This work
H_2-CuCat from Cu-TPA	Bifunctional	–	1	440	0.1 M KBi, 9.2	320	FTO	1
Nitrogen rich-Cu/CuO from Cu-CMP850	Bifunctional	–	1	190	1M KOH; 13.6	135	GC	2
Cu(0)-based leaf-like nanoparticle from Cu–EA	HER	–0.483; 70	1	157	0.1 M PBS; 7	127	FTO	3
Cu(0)-based nanoparticle from Cu(II)-oxime	HER	~ –0.48; 65	1	120	0.5 M PBS; 7.0	63	GC	4
Cu/Cu_2O	HER	–0.443; 30	1.2	217	0.5 M PBS; 7	65	Mo coated glass side	5
Cu_2MoS_4	HER	–0.57; 157	~1.2	300	0.1 M PBS	95	Carbon glassy electrode surface	6

TPA= tris(2-pyridylmethyl)amine, CMP = conjugated mesoporous polymer, EA = ethylenediamine, oxime = [3-(2-(2-hydroxyimino-1-methylpropylideneamino)ethylamino)butan-2-one oxime].

Table S2 Comparison of the OER activities of copper-based electrocatalysts

Catalyst	Type of Catalyst	Onset potential, V *vs*. NHE; overpotential, mV	Current density *j*, mA cm^{-2}	Overpotential mV at the corresponding *j*	Electrolyte; pH	Tafel slope, mV dec^{-1}	Base electrode	Ref.
H_2-Cu_2Cat from **Cu_2L**	Bifunctional	~1.09; ~400	0.1, 1	500, 630	0.1 M NaBi; 9.2	~71.0	FTO	This work
H_2-CuCat from Cu-TPA	Bifunctional	~1.04; 350	0.1, 1	490, 749	0.1 M KBi; 9.2	85	FTO	1
Nitrogen rich-Cu/CuO from Cu-CMP850	Bifunctional		1, 10	350, 450	1M KOH; 13.6	62	GC	2
Cu-Bi	OER	–	0.1, 1	430, 530	0.2 M borate buffer; 9	89.0	FTO	7
$Cu(OH)_2$	OER	~1.16; 470	0.1, 1	550, ~645	0.1 M KBi; 9.2	~78	FTO	8
CuO nanowire annealed CuO	OER	1.03; 340	0.1, 1	430, 550	0.1 M KBi; 9.2	~54.5	FTO	9
Cu_2O	OER	1.04; 350	0.1, 1	430, 490	0.1 M KBi; 9.2	~59.9	FTO	10
CuO nanostructured from Cu-TPA	OER	1.04; 350	0.1, 1	470, 600	0.1 M borate buffer	~56.0	FTO	11
Porous CuO polyhedron from Cu based MOF	OER	1.05; 360	0.1, 1	410, 510	0.1 M KBi; 9.2	75.5	GC and CC	12

Table S2 (continued)

Catalyst	Type of Catalyst	Onset potential, V vs. NHE; overpotential, mV	Current density j, mA cm^{-2}	Overpotential mV at the corresponding j	Electrolyte; pH	Tafel slope, mV dec^{-1}	Base electrode	Ref.
CuO from Cu-TEOA	OER	–	0.1, 1	~560, 800	0.1 M NaOAc; 12.4	130	ITO	13
$CuSO_4$	OER	1.05, 457	2.5	700	1M Na_2CO_3; 10.8	–	ITO	14
$CuO/Cu(OH)_2$	OER	0.983, 390	~2.8	661	1M Na_2CO_3 (NaOH added); 11.7	–	ITO	15
$CuO/Cu(OH)_2$	OER	–	0.1, 1	380, 485	1M Na_2CO_3; 10.8	90	Copper Foil	15
Cu-Nanowire	OER	1.02, 427	~0.6	607	1M Na_2CO_3; 10.8	–	Glass	15
$Cu(OH)_2$	OER		10	610	0.2 M borate buffer; 9	–	Cu foil	16
$Cu(OH)_2$	OER		10	430	0.1 M NaOH	86	Cu foil	16
CuO	OER		10	438	0.1 M NaOH	84	Cu foil	16
CuOx	OER		10	560	0.1 M NaOH	108	Cu foil	16

Table S2 (continued)

Catalyst	Type of Catalyst	Onset potential, V vs. NHE; overpotential, mV	Current density *j*, mA cm^{-2}	Overpotential mV at the corresponding *j*	Electrolyte; pH	Tafel slope, mV dec^{-1}	Base electrode	Ref.
$Cu(OH)_2$/ CuO	OER	~0.9; ~380	0.1, 1	~475, 540	0.2 M phosphate buffer; 12	62	ITO	17
Annealed CuO	OER	–	0.1, 1	360, 430	1 M KOH	61.4	FTO	18
CuO from Cu-EA	OER	–	1	370	1 M KOH; 13.6	~90	FTO	19
CuO from Cu-Py	OER	~1.04; 459	0.2	819	0.1 M phosphate buffer; 11	–	FTO	20
H_2O_2-treated CuO	OER	~0.80; 340	–	–	0.1 M KOH	–	GC	21
$CuO/Cu(OH)_2$ from Cu^{II}-Gly	OER	–	0.1, 1	380, 450	0.2 M phosphate buffer; 12	~64	ITO	22

TPA= tris(2-pyridylmethyl)amine; TEOA= triethanolamine; CMP = conjugated mesoporous polymer EA= ethylenediamine; Py= (*E*)-3-(pyridine-2-yldiazenyl)naphthalene-2-ol; Gly=glycine.

References

1 X. Liu, H. Zheng, Z. Sun, A. Han and P. Du, *ACS Catal.*, 2015, **5**, 1530−1538.
2 S. Cui, M. Qian, X. Liu, Z. Sun and P. Du, *ChemSusChem*, 2016, **9**, 2365–2373.
3 X. Liu, S. Cui, Z. Sun and P. Du, *Chem. Commun.*, 2015, **51**, 12954–12957.
4 J. Du, J. Wang, L. Ji, X. Xu and Z. Chen, *ACS Appl. Mater. Interfaces*, 2016, **8**, 30205−30211.
5 J. Zhao, P. D. Tran, Y. Chen, J. S. C. Loo, J. Barber and Z. J. Xu, *ACS Catal.*, 2015, **5**, 4115−4120.
6 P. D. Tran, M. Nguyen, S. S. Pramana, A. Bhattacharjee, S. Y. Chiam, J. Fize, M. J. Field, V. Artero, L. H. Wong, J. Loo and J. Barber, *Energy Environ. Sci.*, 2012, **5**, 8912−8916.
7 F. Yu, F. li, B. Zhang, H. Li and L. Sun, *ACS Catal.*, 2015, **5**, 627−630.
8 S. Cui, X. Liu, Z. Sun and P. Du, *ACS Sustainable Chem. Eng.*, 2016, **4**, 2593−2600.
9 X. Liu, S. Cui, Z. Sun and P. Du, *Electrochim. Acta*, 2015, **160**, 202–208.
10 X. Liu, Z. Sun, S. Cui and P. Du, *Electrochim. Acta*, 2016, **187**, 381–388.
11 X. Liu, H. Jia, Z. Sun, H. Chen, P. Xu and P. Du, *Electrochem. Commun.*, 2014, **46**, 1–4.
12 T.-T. Li, J. Qian and Y.-Q. Zheng, *RSC Adv.*, 2016, **6**, 77358–77365.
13 T.-T. Li, S. Cao, C. Yang, Y. Chen, X.-J. Lv and W.-F. Fu, *Inorg. Chem.*, 2015, **54**, 3061–3067.
14 Z. Chen and T. J. Meyer, *Angew. Chem. Int. Ed.*, 2013, **52**, 700–703.
15 J. Du, Z. Chen, S. Ye, B. J. Wiley and T. J. Meyer, *Angew. Chem. Int. Ed.*, 2015, **54**, 2073 –2078.
16 C.-C. Hou, W.-F. Fu and Y. Chen, *ChemSusChem*, 2016, **9**, 2069–2074.
17 C. Lu, J. Du, X.-J. Su, M.-T. Zhang, X. Xu, T. J. Meyer and X. Chen, *ACS Catal.*, 2016, **6**, 77−83.
18 X. Liu, S. Cui, Z. Sun, Y. Ren, X. Zhang and P. Du, *J. Phys. Chem. C*, 2016, **120**, 831−840.
19 X. Liu, S. Cui, M. Qian, Z. Sun and P. Du, *Chem. Commun.*, 2016, **52**, 5546–5549.
20 M. M. Najafpour, F. Ebrahimi, R. Safdari, M. Z. Ghobadi, M. Tavahodi and P. Rafighi, *Dalton Trans.*, 2015, **44**, 15435–15440.
21 A. D. Handoko, S. Deng, Y. Deng, A. W. F. Cheng, K. W. Chan, H. R. Tan, Y. Pan, E. S. Tok, C. H. Sow and B. S. Yeo, *Catal. Sci. Technol.*, 2016, **6**, 269–274.
22 C. Lu, J. Wang and Z. Chen, *ChemCatChem*, 2016, **8**, 2165 – 2170.